J Mater Sci: Mater Electron (2017) 28:1211–1216
DOI 10.1007/s10854-016-5647-2

# Improved piezoelectricity and high strain response of $(1 - x)(0.948K_{0.5}Na_{0.5}NbO_3 - 0.052LiSbO_3) - xBi_2O_3$ ceramics

**Yan Zhao[1] · Zhijun Xu[1] · Ruiqing Chu[1] · Jigong Hao[1] · Juan Du[1] · Guorong Li[2]**

Received: 3 July 2016 / Accepted: 29 August 2016 / Published online: 15 September 2016


**Abstract** $(1 - x)(0.948K_{0.5}Na_{0.5}NbO_3 - 0.052LiSbO_3) - xBi_2O_3$ ($x = 0.001 \sim 0.004$) (abbreviated as KNN − 5.2LS − $x$Bi) lead-free piezoelectric ceramics were prepared using conventional solid sintering method and the effect of bismuth oxide ($Bi_2O_3$)-doping on phase structure, microstructure and electric properties were investigated. It was found that $Bi_2O_3$-doping induces a phase transition from the tetragonal phases to a pseudocubic phase with a normal-relaxor ferroelectric transformation, and acts as grain growth inhibitor, which significantly decreases the grain size of the ceramics. The KNN − 5.2LS ceramic with 0.2 *mol.* % $Bi_2O_3$ exhibited the optimum electrical properties ($d_{33} = 229$ pC/N, $k_p = 31.08$ %), together with a low $T_{O-T}$ of 77 °C. In addition, the highest $T_C$ (~355 °C), the highest $S_{max}$ (~0.20 %) and $d_{33}$* (~392 pm/V) values can be attained in the ceramics with $x = 0.001$, which is superior to those of the previously reported KNN-based ceramics. These results show that the KNN − 5.2LS − $x$Bi ceramic is one of the most promising candidates for replacing PZT-based ceramics.

## 1 Introduction

Piezoceramics are always one of the most important and widely used materials, and the related researches are becoming a forefront of high-technology advanced materials [1–7]. Since the 1950s, $PbZr_{1-x}Ti_xO_3$ (PZT)-based ceramics have drawn much attention due to their excellent piezoelectric properties. However, the lead content (~60 *wt.*%) of PZT raises environmental concerns during their preparation, process, and even disposal. As a result, there is an increasing interest in developing lead-free piezoelectrics with the aim of achieving an equivalent or even higher piezoelectric response as those of the lead-based ones.

Among the lead-free piezoelectric materials, $(K_{0.5}Na_{0.5})NbO_3$ (abbreviated as: KNN) ceramic is considered to be one of the promising candidates owing to their relatively high Curie temperature ($T_C$) and moderate piezoelectric response [3, 4, 8, 9]. To date, most of the research has focused on KNN ceramics [4, 10–15]. For example, a remarkable achievement in $d_{33}$ (~416 pC/N) can be gained in the KNN ceramics doped by Ta, Sb, and Li via the complicated reaction template grain growth (RTGG) method [4]. Since then, KNN has become one of the most extensively investigated lead-free piezoelectric systems [16, 17]. The major disadvantage of pure KNN, however, is difficulties in obtaining sufficiently dense ceramics by conventional sintering in air [18]. In order to improve the densification and piezoelectric properties of KNN-based ceramics, specialized sintering processes, such as hot pressing and spark plasma sintering processes(SPS), have been introduced for preventing the volatility of alkali elements and to lower the sintering temperature to overcome the drawback of insufficient density [19]. But the cost of these methods is high and the preparation technology is complex, which is not favorable to the industrialization of KNN ceramics preparation process. Now, numerous compositional engineering approaches have been explored to optimize the piezoelectric properties of KNN materials like adding $BaTiO_3$ [20], $SrTiO_3$ [21], $LiNbO_3$ [22], $LiTaO_3$ [23], and $LiSbO_3$ [24] to form new solid solutions.

✉ Zhijun Xu
zhjxu@sohu.com; zhjxu@lcu.edu.cn

[1] College of Materials Science and Engineering, Liaocheng University, Liaocheng 252059, People's Republic of China

[2] The State Key Lab of High Performance Ceramics and Superfinemicrostructure, Shanghai Institute of Ceramics, Chinese Academy of Science, Shanghai 200050, People's Republic of China

Although some significant breakthroughs have been achieved in the study of KNN-based piezoelectrics, there was certain gap compared with lead-based materials. The good electric properties of lead-based ceramics have a close relationship with the electronic structure of Pb [25]. And researches show that Bi has the same electronic distribution, similar ionic radius and the molecular weight with Pb, which is adjacent in periodic table of elements [26]. The strong ferroelectricity of $(Bi_{1/2}Na_{1/2})TiO_3$ is derived from $(Bi_{1/2}Na_{1/2})^{2+}$ ion, especially $Bi^{3+}$ ion, so Bi also can promote the generation of strong ferroelectricity. Meanwhile, lead 6 *s* and O 2*p* states are strongly hybridized, which played a great role in piezoresponse of lead-based ceramics, and the hybridization leads to a large strain that stabilizes the tetragonal phase [27]. In addition, $Bi^{3+}$ and $Pb^{2+}$ have the same extranuclear structure $6s^26p^0$, $Bi^{3+}$ empty $6p^0$ states can strongly hybridize with the $O^{2-}$ $2p^6$ states to form the Bi–O bonding, therefore, the perovskite solid solution containing $Bi^{3+}$ can show high piezoelectric and ferroelectric response, such as $BiMeO_3$–$PbTiO_3$ [28]. In this study, we selected $0.948(K_{0.5}Na_{0.5})$-$NbO_3 - 0.052LiSbO_3$, which is known to have excellent piezoelectric properties with the polymorphic phase transition (PPT) at room-temperature, as a base material with small amounts of $Bi_2O_3$ being introduced as doping species. The influences of $Bi_2O_3$ on the phase structure, microstructure and electrical properties of the ceramics were investigated.

## 2 Materials and methods

$(1 - x)(0.948K_{0.5}Na_{0.5}NbO_3 - 0.052LiSbO_3) - xBi_2O_3$ (abbreviated as: $KNN - 5.2LS - x$Bi, $x = 0 \sim 0.004$) piezoelectric ceramics were prepared by conventional solid-state reaction method using $Na_2CO_3$ (99.8 %), $K_2CO_3$ (99 %), $Li_2CO_3$ (98 %), $Nb_2O_5$ (99.96 %), $Sb_2O_3$ (99 %), $Bi_2O_3$ (99.64 %) as starting materials. The starting materials were mixed by ball-milling for 12 h in ethanol with zirconia balls as milling media. The slurries were dried and calcined at 850 °C for 2 h. After calcination, the mixtures were milled again for 12 h. The obtained powders were pressed to form disks using 8 *wt.%* polyvinyl alcohol (PVA) as a binder, and pressed into pallets with a diameter of 12 mm and a thickness of 1.0 mm under a pressure of about 200 MPa. After burning off PVA, the ceramics were sintered at 1110 °C for 2 h in air.

The crystal structures of the sintered ceramics were determined by X-ray powder diffraction analysis (XRD) (D8 Advance, Bruker Inc. Germany). The surface morphology of the ceramics was studied by scanning electron microscope (SEM) (JSM-6380, Japan). For the electrical measurements, silver paste was coated on both sides of the sintered samples and fired at 740 °C for 20 min to produce electrodes. The temperature dependences of the dielectric properties were measured using a broadband dielectric spectrometer (Novocontrol Germany). The electric-field-induced polarization (*P–E*) and strain (*S–E*) measurements were carried out using an aix-ACCT TF2000FE-HV ferroelectric test unit (aix-ACCT Inc. Germany). The piezoelectric measurements were carried out using a quasi-static $d_{33}$-meterYE2730 (SINOCERA, China). Before the measurement, the samples were poled in silicon oil at room temperature under 50–70 kV $cm^{-1}$ for 20 min. The planar electromechanical coupling factor $k_p$ was calculated using the following equations with an impedance analyzer (Agilent 4294A) [29]:

$$\frac{1}{k_p^2} = 0.395\frac{f_r}{f_a - f_r} + 0.574 \quad (1)$$

where $f_r$ and $f_a$ are the resonance frequency and the anti-resonance frequency, respectively.

## 3 Results and discussion

Figure 1a shows the XRD patterns of $KNN - 5.2LS - x$Bi ceramics in the $2\theta$ range of 20–70°. A stable solid solution among KNN, LS, and Bi with a pure perovskite structure without any secondary phase is formed in all indicated compositions, indicating that $Bi^{3+}$ ions are successfully diffused into the $KNN - 5.2LS$ lattice. Ceramics with $x \leq 0.003$ possess a tetragonal structure with the splitting of the (001)/(100) and (002)/(200) characteristic peaks [30]. However, at ceramics with $x > 0.003$, the split peaks around 52° are gradually combined into one single peak, suggesting that the ceramic transforms into pseudo-cubic structure at high contents of $Bi_2O_3$ [31]. Figure 1b shows the variation of lattice parameters and the cell volume as functions of *x*. The lattice parameters are calculated by lattice parameter calculation software from the XRD patterns. The cell volume of the ceramics with adding $Bi_2O_3$ are smaller than that of pure $KNN - 5.2LS$ ceramics due to the smaller ionic radii of $Bi^{3+}$ (1.32 Å, CN = 12) than those of A-site $K^+$ (1.64 Å, CN = 12) or $Na^+$ (1.39 Å, CN = 12) [32]. Therefore, $Bi^{3+}$ enter into the A-site of KNN to substitute for $K^+$ and $Na^+$ because of radius matching, resulting in the lattice deformation.

Figure 2 displays the surface morphologies of the $KNN - 5.2LS - x$Bi ceramics. The microstructure appears homogeneous without any apparent second phase. The average grain size decreases monotonically as the $Bi_2O_3$ content increases, indicating that the role of $Bi_2O_3$ in $KNN - 5.2LS - x$Bi system is a grain growth inhibiter [33]. When $x = 0.004$, some pores are formed in the interior of the grains, this may because $Bi_2O_3$ can form a

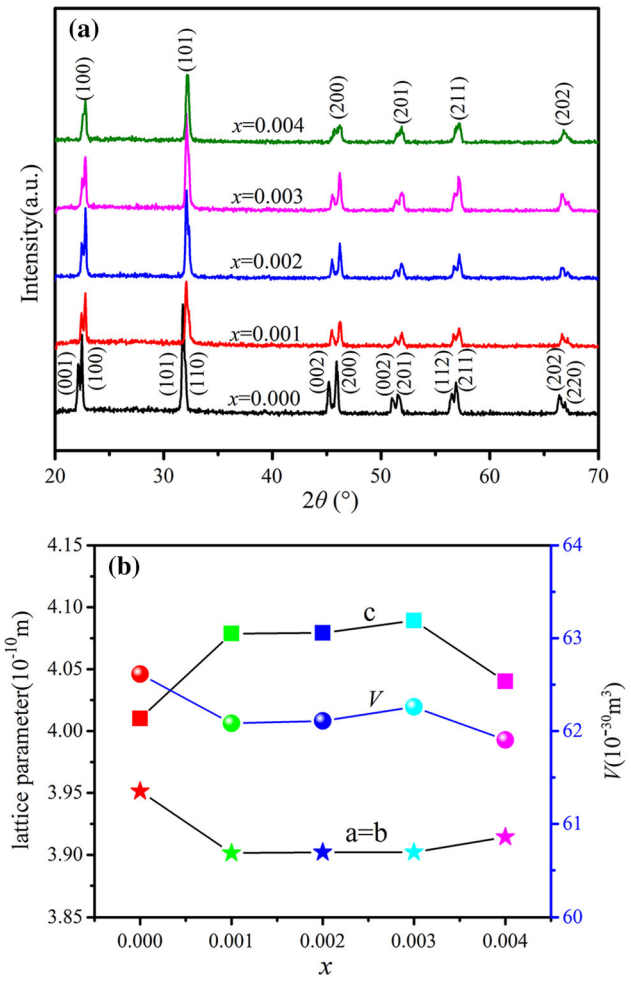


**Fig. 1** **a** XRD patterns of KNN − 5.2LS − *x*Bi ceramics in the $2\theta$ range of 20°–70°, **b** the variation of lattice parameters and the cell volume as functions of *x*

liquid phase in the KNN-based ceramics at 690 °C, and some gases couldn't discharge timely while they are surrounded by grain boundary to form pores in the process of grain boundary migration [34].

Figure 3a shows temperature dependence of dielectric permittivity $\varepsilon_r$ for KNN − 5.2LS − *x*Bi samples at a measuring frequency of 10 kHz, and Fig. 3b plots the phase diagram of the KNN − 5.2LS − *x*Bi ceramics, which summarized from the temperature dependence of the dielectric behavior in Fig. 3a. As *x* increases, the $T_C$ increases and then decreases while $T_{O-T}$ reaches the lowest at $x = 0.002$ as illustrated in Fig. 3b. Ceramics with $x \leq 0.003$ have two phase transitions, which are from orthorhombic to tetragonal polymorphic phase ($T_{O-T}$) and from tetragonal polymorphic phase to cubic phase ($T_C$) respectively [22]. Here, we note that a little inconsistency is seen between the $T_{O-T}$ results obtained through the dielectric measurement and the results acquired from XRD analysis. While the $\varepsilon_r$ versus temperature curves show that their crystalline structures should be of orthorhombic symmetry, the actual crystalline structures are of tetragonal symmetry. The actual $T_{O-T}$ for the samples should be lower than 80 °C due to the thermal hysteresis since dielectric permittivity is measured during a heating process [35]. Such inconsistency is speculated to arise from a state change of phase coexistence with temperature around $T_{O-T}$ in the dielectric measurement. While XRD characterizes directly the crystalline structure in a quasi-equilibrium or equilibrium state, the $\varepsilon_r$ versus temperature curves give indirectly the information of the state change of phase coexistence. The states of phase coexistence during a heating or cooling process may not always be quasi-

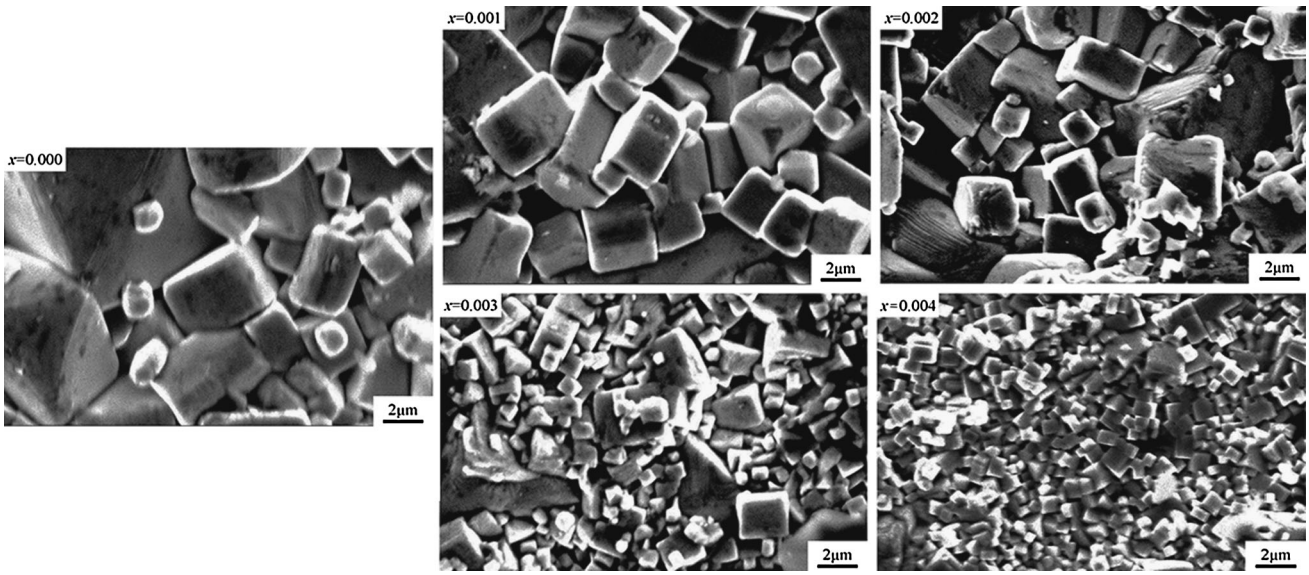


**Fig. 2** SEM micrographs of KNN − 5.2LS − *x*Bi ceramics sintered at 1110 °C for 2 h

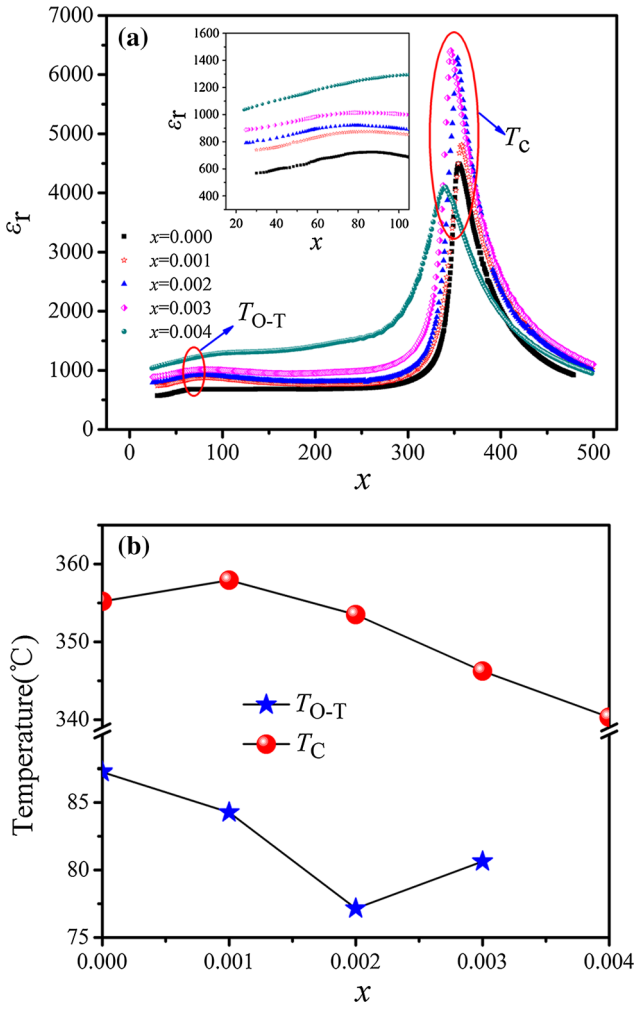


**Fig. 3** **a** Temperature dependence of dielectric permittivity for KNN − 5.2LS − *x*Bi samples at a measuring frequency of 10 kHz, **b** compositional dependence of $T_C$ and $T_{O-T}$ as a function of *x* for KNN − 5.2LS − *x*Bi

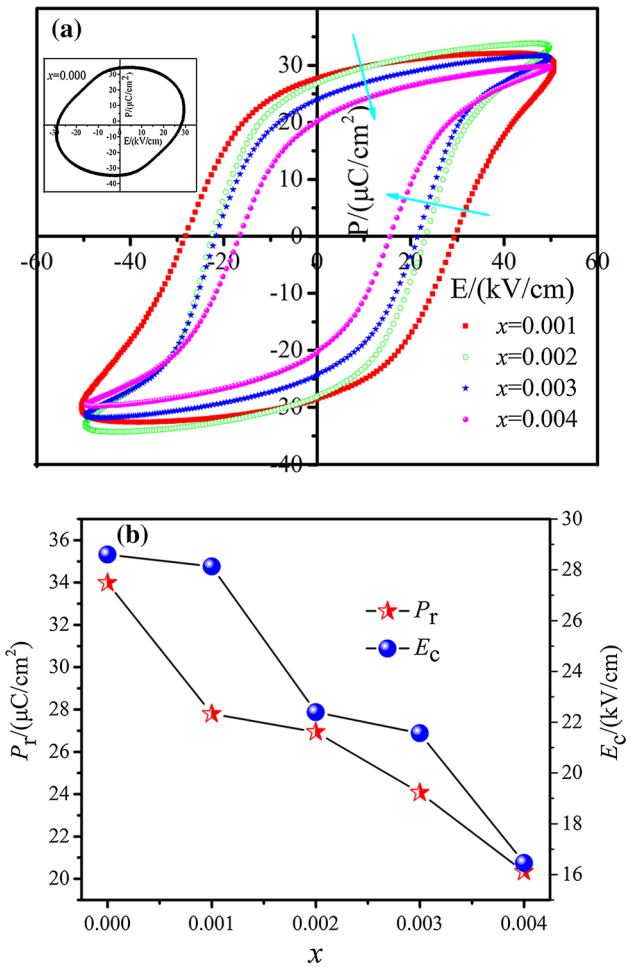


**Fig. 4** **a** *P–E* hysteresis loops of KNN − 5.2LS − *x*Bi samples measured at 10 Hz and room temperature, **b** $P_r$ and $E_c$ variations of the KNN − 5.2LS − *x*Bi ceramics as a function of *x*

equilibrium or equilibrium because time is needed for the adjustment of domain structure inside the grains to follow the temperature change [36]. Similar inconsistencies were previously found also in some other KNN-based ceramics [37, 38]. For samples with $x > 0.003$, the $T_{O-T}$ of the ceramics disappears, and only the cubic-tetragonal phase transition is observed above room temperature. This result corresponds with the XRD-pattern, as shown in Fig. 1. Moreover, it was found that the dielectric maxima drops down rapidly and the dielectric peaks become extremely broad with the excess of $Bi_2O_3$, which should be ascribed to the formation of pseudo-cubic structures at high level of Bi substitution [39].

Figure 4a shows the ferroelectric *P–E* hysteresis loops of KNN − 5.2LS − *x*Bi ceramics measured at room temperature and 10 kHz. Round-shaped *P–E* hysteresis loops are obtained in the pure sample due to a relative large leakage current [40]. However, the samples with adding $Bi_2O_3$ exhibit a good square-shaped hysteresis loop, which are typical for ferroelectrics [41]. In order to further understand the ferroelectric properties, the response of their remnant polarization ($P_r$) and coercive field ($E_C$) as a function of *x* is provided in Fig. 4b. It can be seen that both $P_r$ and $E_C$ decreases gradually with increasing $Bi_2O_3$ content. Increasing amount of $Bi_2O_3$ leads to more defects in the KNN − 5.2LS lattice, which hinder the switching of the domains and cause poor $P_r$. The decrease of $E_C$ values may be due to the "soft" effect of $Bi_2O_3$, which reduces oxygen vacancies to maintain the charge neutrality and facilitates the poling process of the ceramics [42]. The $x = 0.002$ ceramic presents $P_r$ of 26.94 μC/cm$^2$ and $E_C$ of 22.39 kV/cm, showing relatively excellent ferroelectric properties.

Figure 5 shows the composition dependence of the piezoelectric coefficient ($d_{33}$) and electromechanical coupling factor ($k_p$) of the KNN − 5.2LS − *x*Bi ceramics.

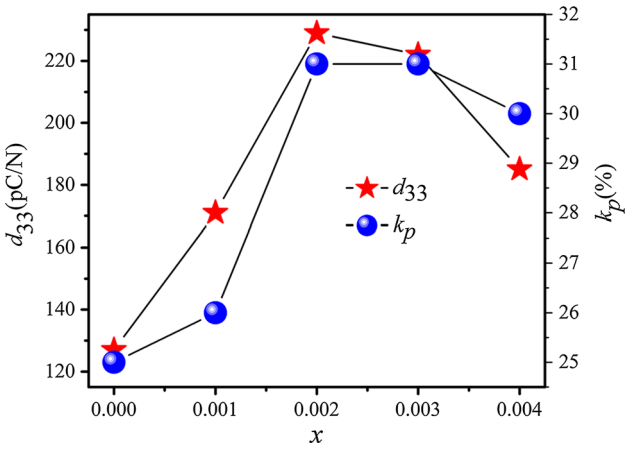


**Fig. 5** Piezoelectric constant $d_{33}$ and the planar electromechanical coefficient $k_p$ of the KNN − 5.2LS − $x$Bi ceramics as a function of $x$

Both $k_p$ and $d_{33}$ gradually increased and then decreased with increasing $Bi_2O_3$ content, giving a maximum value of 31.08 % and 229 pC/N at $x = 0.002$. It is seen that addition of small amounts of $Bi_2O_3$ yields to large electrical properties. The promotion may be attributed to three reasons. Firstly, the orthorhombic to tetragonal phase transition temperature at $x = 0.002$ is lower, which makes the two phase regions gradually approach room temperature [40]. Secondly, the $Bi_2O_3$ modification in KNN − 5.2LS softens the materials. So the KNN − 5.2LS − $x$Bi ceramic is thought to have more extrinsic contribution in the piezoelectric coefficient when compared with pure KNN − 5.2LS. Finally, the optimum $Bi_2O_3$ addition and the optimum sintering temperature can improve the density of the ceramics, which has positive effects on the electrical properties. However, with the high addition of $Bi_2O_3$ ($x > 0.002$) the variation of electrical properties as the function of $x$ could be attributed to the competing effects of grain size, porosity and so forth [43].

Figure 6a shows the bipolar strain curves of KNN − 5.2LS − $x$Bi ceramics measured at RT and 10 Hz. All ceramics show butterfly-shaped strain hysteresis loops with visible negative strain $S_{neg}$ (the definition for $S_{neg}$ can be found in our previous work [44]), which is typical for ferroelectrics [41]. The $d_{33}$* can be calculated from the slop of the electric-field-induced strain using the following equation: $d_{33}^* = S_{max}/E_{max}$. Both $S_{max}$ and $d_{33}$* of KNN − 5.2LS − $x$Bi ceramics are presented in Fig. 6b as a function of $x$. The $S_{max}$ and $d_{33}$* obtain a similar changed trend as the contents of $Bi_2O_3$ increase. More importantly, the $S_{max}$ (∼0.20 %) and $d_{33}$* (∼392 pm/V) values can be attained in the ceramics with $x = 0.001$, which are much higher than that of pure KNN − 5.2LS (0.07 % and 133 pm/V). In addition, the $S$–$E$ curve of samples exhibits a transition from the butterfly shape to horn shape with the decrease of the $S_{neg}$ with $x \geq 0.001$,

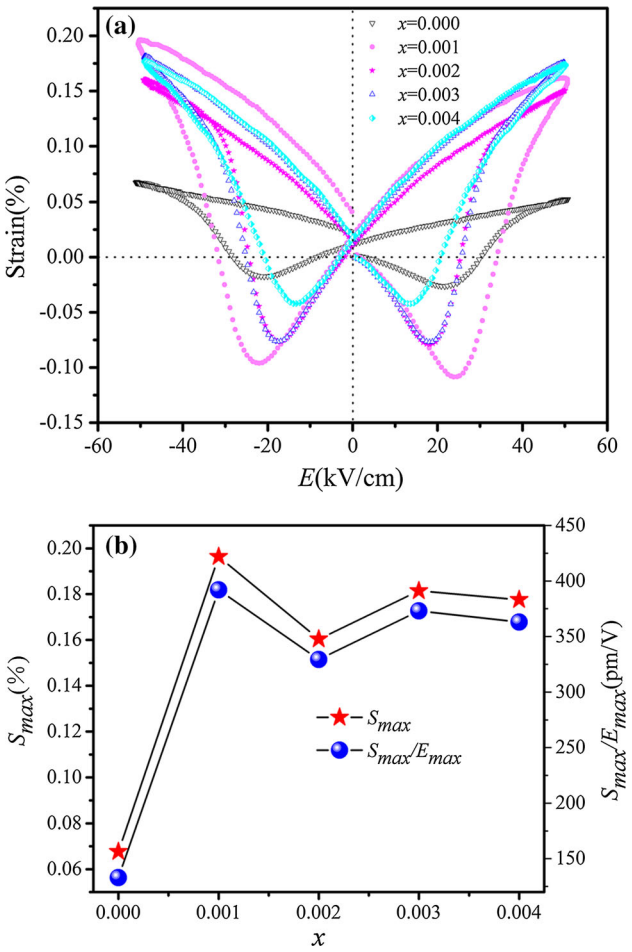


**Fig. 6** **a** bipolar strain curves of KNN − 5.2LS − $x$Bi ceramics measured at RT and 10 Hz, **b** maximum value of the strain and $d_{33}$* of the ceramics as a function of $x$

suggesting phase structure transition from the tetragonal phases to a pseudocubic symmetry, which indicates the development of ergodic relaxor phase at zero electric field. This indicated that the electrically induced strain were mainly associated with external contribution (domain wall motion) and little from contribution from material intrinsic piezoelectric effect [45]. This results match well with the ferroelectric properties in Fig. 5. This also confirms that the high electrically induced strain of KNN-based ceramics is based on the expense of the electric properties.

## 4 Conclusion

$(1 - x)(0.948K_{0.5}Na_{0.5}NbO_3 - 0.052LiSbO_3) - xBi_2O_3$ lead-free piezoelectric ceramics were prepared using conventional solid sintering method and the effects of $Bi_2O_3$ on the phase structure, microstructure and electrical properties of the ceramics were systematically studied. All compositions had a pure perovskite structure.

And ceramics with $x > 0.003$ transform into pseudo-cubic structure. The average grain size decreases monotonically as the $Bi_2O_3$ content increases, implies that the role of $Bi_2O_3$ in KNN − 5.2LS system is a grain growth inhibiter. Enhanced electrical properties ($d_{33} = 229$ pC/N, $k_p = 31.08$ % and $T_{O-T} = 77$ °C) were achieved at $x = 0.002$. In addition, there are the highest $T_C$ of 355 °C and the highest strain value of 0.20 % ($S_{max}/E_{max} = 392$ pm/V) in the ceramics with $x = 0.001$, which is superior to those of the previously reported KNN-based ceramics. In consequence, The proper amount of $Bi_2O_3$ can actively improve the electric properties of the KNN − 5.2LS − $x$Bi ceramics, suggesting that this material should be an attractive lead-free material for piezoelectric applications.

**Acknowledgments** This work was supported by the National High Technology Research and Development Program of China (No. 2016YFB0402701), National Natural Science Foundation of China (No. 51372110, 51402144, 51302124, 51302025), Science and Technology Planning Project of Guangdong Province, China (No. 2013B091000001), Independent innovation and achievement transformation in Shandong Province special, China (No. 2014CGZH0904), The Project of Shandong Province Higher Educational Science and Technology Program (No. J14LA11, No. J14LA10), Research Foundation of Liaocheng University (No. 318011301, No. 318011306).

## References

1. J.U. Rahman, A. Hussain, A. Maqbool, T.K. Song, W.J. Kim, S.S. Kim, M.H. Kim, Curr. Appl. Phys. **14**, 331 (2014)
2. T.R. Shrout, S. Zhang, J. Electriceram. **19**, 111 (2007)
3. L. Egerton, D.M. Dillon, J. Am. Ceram. Soc. **42**, 438 (1959)
4. Y. Saito, H. Takao, T. Tani, T. Nonoyama, K. Takatori, T. Homma, T. Nagaya, M. Nakamura, Nature **432**, 84 (2004)
5. J.G. Wu, D.Q. Xiao, J.G. Zhu, Chem. Rev. **115**, 2559 (2015)
6. J. Rodel, W. Jo, K. Seifert, E.M. Anton, T. Granrow, D. Damjanovic, J. Am. Ceram. Soc. **89**, 1153 (2009)
7. D. Damjanovic, N. Klein, J. Li, V. Porokhonskyy, Funct. Mater. Lett. **3**, 5 (2010)
8. B. Jaffe, W.R. Cook, H. Jaffe, *Piezoelectric Ceramics* (Academic, New York, 1971)
9. E. Ringgaard, T. Wurlitzer, W.W. Wolny, Ferroelectrics **319**, 97 (2005)
10. Y.P. Guo, K. Kakimoto, H. Ohsato, Appl. Phys. Lett. **85**, 4121 (2004)
11. S. Zhang, R. Xia, T.R. Shrout, G. Zang, J. Wang, J. Appl. Phys. **100**, 104108 (2006)
12. Y. Gao, J.L. Zhang, Y.L. Qing, Y.Q. Tan, Z. Zhang, X.P. Hao, J. Am. Ceram. Soc. **94**, 2968 (2011)
13. B.Y. Zhang, J.G. Wu, X.J. Cheng, X.P. Wang, D.Q. Xiao, J.G. Zhu, X.J. Wang, X.J. Lou, ACS Appl. Mater. Inter. **5**, 7718 (2013)
14. Z. Wang, D.Q. Xiao, J.G. Wu, M. Xiao, F.X. Li, J.G. Zhu, J. Am. Ceram. Soc. **97**, 688 (2014)
15. T. Zheng, J.G. Wu, X.J. Cheng, X.P. Wang, B.Y. Zhang, D.Q. Xiao, J.G. Zhu, X.J. Lou, X.J. Wang, Dalton Trans. **43**, 11759 (2014)
16. B.Q. Ming, J.F. Wang, P. Qi, G.Z. Zang, J. Appl. Phys. **101**, 4103 (2007)
17. Y.X. Liu, Y.Q. Huang, T.T. Liu, B. Zhang, Q.S. Yan, G.X. Zhang, J. Mater. Sci. **45**, 188 (2010)
18. C. Wang, J. Chen, H.L. Chen, Y.D. Hou, M.K. Zhu, J. Inorg. Mater. **30**, 59 (2015)
19. R.P. Wang, R.J. Xie, T. Sekiya, Y. Shimojo, Mater. Res. Bull. **39**, 1709 (2004)
20. Y. Guo, K. Kakimoto, H. Ohsato, Jpn. J. Appl. Phys. **43**, 6662 (2004)
21. Y. Guo, K. Kakimoto, H. Ohsato, Solid State Commun. **129**, 279 (2004)
22. Y. Guo, K. Kakimoto, H. Ohsato, Appl. Phys. Lett. **85**, 4121 (2004)
23. Y. Guo, K. Kakimoto, H. Ohsato, Mater. Lett. **59**, 241 (2005)
24. S.J. Zhang, R. Xia, H. Hao, H.X. Liu, T.R. Shrout, Appl. Phys. Lett. **92**, 152904 (2008)
25. A.F. Tian, Z.P. Xu, S.J. Liu, N. Jiang, H.L. Du, J. Chin. Ceram. Soc. **42**, 667 (2014)
26. C.R. Zhou, X.Y. Liu, Mater. Chem. Phys. **108**, 413 (2008)
27. R.E. Cohen, Nature **358**, 136 (1992)
28. R.E. Eitel, C.A. Randall, T.R. Shrout, P.W. Rehrig, W. Hackenberger, S.E. Park, Jpn. J. Appl. Phys. **40**, 5999 (2001)
29. R.C. Chang, S.Y. Chu, Y.F. Lin, C.S. Hong, P.C. Kao, C.H. Lu, Sens. Actuators A Phys. **138**, 355 (2007)
30. F. Tang, H. Du, D. Liu, F. Luo, W. Zhou, J. Inorg. Mater. **2**, 323 (2007)
31. Z.P. Yang, Y.F. Chang, L.L. Wei, Appl. Phys. Lett. **90**, 042911 (2007)
32. Q.W. Zhang, H.Q. Sun, X.S. Wang, T. Zhang, Mater. Lett. **117**, 283 (2014)
33. C. Xu, D. Lin, K.W. Kwok, Solid State Sci. **10**, 934 (2008)
34. D.J. Liu, H.L. Du, F.S. Tang, F. Luo, W.C. Zhou, J. Chin. Ceram. Soc. **35**, 1141 (2007)
35. R.Z. Zuo, J. Fu, X.H. Wang, L.T. Li, J. Mater. Sci.: Mater. Electron. **21**, 519 (2010)
36. Y. Gao, J.L. Zhang, Y.L. Qing, Y.Q. Tan, Z. Zhang, X.P. Hao, J. Am. Ceram. Soc. **94**, 2968 (2011)
37. Y. Saito, H. Takao, Ferroelectrics **338**, 1433 (2006)
38. L. Wu, J.L. Zhang, P. Zheng, C.L. Wang, J. Phys. D Appl. Phys. **40**, 3527 (2007)
39. J.G. Hao, Z.J. Xu, R.Q. Chu, W. Li, G.R. Li, Q.R. Yin, J. Alloys Compd. **484**, 233 (2009)
40. J. Du, F. An, Z.J. Xu, R.F. Cheng, R.Q. Chu, X.J. Yi, J.G. Hao, W. Li, Ceram. Int. **42**, 1943 (2016)
41. J.G. Hao, B. Shen, J.W. Zhai, H. Chen, J. Am. Ceram. Soc. **97**, 1776 (2014)
42. K.J. Zhu, D.L. Wang, B. Shao, J.H. Qiu, H.L. Ji, J. Chin. Ceram. Soc. **39**, 1928 (2011)
43. Y.J. Zhao, X.Y. Yuan, Y.Z. Zhao, H.P. Zhou, J.B. Li, H.B. Jin, Mater. Lett. **162**, 226 (2016)
44. J.G. Hao, W.F. Bai, W. Li, B. Shen, J.W. Zhai, J. Appl. Phys. **114**, 044103 (2013)
45. C.G. Ye, J.G. Hao, S. Shen, J.W. Zhai, J. Am. Ceram. Soc. **95**, 3577 (2012)